MULTISCALE MODELING OF THE
ACOUSTIC PROPERTIES OF LUNG PARENCHYMA [*]

MALIN SIKLOSI[1], OLIVER E. JENSEN[2], RICHARD H. TEW[2] AND ANDERS LOGG[3]

Abstract. Lung parenchyma is a foam-like material consisting of millions of alveoli. Sound transmission through parenchyma plays an important role in the non-invasive diagnosis of many lung diseases. We model the parenchyma as a porous solid with air filled pores and consider the Biot equations as a model for its acoustic properties. The Biot equations govern small-amplitude wave propagation in fluid-saturated porous solids, and include the effects of relative motion between the fluid and the solid frame. The Biot equations can be derived from a micro-structure model of the porous material, and the material parameters in the equations can be obtained from the solution of two independent micro-structure problems, a fluid-cell problem (governed by the unsteady Stokes equations) and a solid-cell problem. We review the homogenization approach for media with periodic micro-structure, and solve a fluid-cell problem numerically for an idealized two-dimensional micro-scale geometry for a wide range of frequencies. We also discuss sound speeds in lung tissue.

Résumé. ...

1. INTRODUCTION

Lung sounds provide an invaluable non-invasive technique for the assessment and diagnosis of a wide range of pulmonary pathologies [33]. In addition to the traditional use of a stethoscope in the doctor's surgery, acoustic devices can be used to measure lung properties (such as volume) or to monitor a patient's respiratory condition. While clinicians may have a good empirical understanding of the relationship between the character of a lung sound and the underlying pathology, less is known about the detailed physical mechanisms of sound generation and transmission in lung tissue, and the relationship between sounds and any underlying lung diseases.

The lung is a complex organ. The airways of the lung form a bifurcating network of tubes that is embedded in parenchyma, a foam-like material consisting of around 300 million alveoli. Diseases such as asthma, emphysema, and COPD (chronic obstructive pulmonary disease) are associated with changes in the detailed structure of the lung at the alveolar level. Many experimental studies have been performed on healthy and diseased lungs in order to investigate the acoustic properties of the parenchyma and to assess to what extent it is possible to obtain information on tissue properties from acoustic measurements. However, current theoretical models of

[1] Center for Biomedical Computing, Simula Research Laboratory, P.O.Box 134, 1325 Lysaker, Norway, e-mail: `malinsi@simula.no`

[2] School of Mathematical Sciences, University of Nottingham, University Park, Nottingham NG7 2RD, UK,
e-mail: `Oliver.Jensen@nottingham.ac.uk` & `Richard.Tew@nottingham.ac.uk`

[3] Center for Biomedical Computing, Simula Research Laboratory / Department of Informatics, University of Oslo, P.O.Box 134, 1325 Lysaker, Norway, e-mail: `logg@simula.no`

the acoustic properties of parenchyma are relatively simple and are based on the work by Rice [36], where the parenchyma is modelled as a homogeneous mixture of a gas phase and a tissue phase. Further development of theoretical models which are based on more detailed tissue mechanics therefore has the potential to contribute to increased understanding of experimental findings, and is the purpose of this paper. For an overview of experimental and theoretical studies, we refer to [33]. Also, for recent developments of homogeneous mixture models, see [28–30].

In [36], Rice suggested a model for the speed of sound in lung parenchyma which is based on the fact that a two-phase porous medium may be considered to be an elastic continuum if the sound wavelength greatly exceeds the pore size and if the cells do not communicate [40]. Under these assumptions the speed of sound in the medium is independent of frequency and is given by the expression

$$V_{\text{Wood}} = \sqrt{K_{\text{ave}}/\rho_{\text{ave}}}, \tag{1}$$

where K_{ave} is the average bulk modulus and ρ_{ave} is the average density of the mixture. Expression (1) is often called Wood's formula. In [36] it is assumed that the communication between alveoli is negligible. The alveolar diameter is about 10^{-4} m and the speed of sound in parenchyma is of the order 30 m/s. Hence, Rice modeled the parenchyma as a homogeneous mixture of non-communicating air bubbles, modeling the alveoli, and water, modeling the lung tissue. For this model the speed of sound is given by equation (1) and

$$K_{\text{ave}} = \left(\frac{\phi}{\kappa} + \frac{(1-\phi)}{K_s} \right)^{-1}, \quad \rho_{\text{ave}} = \phi \rho_f + (1-\phi)\rho_s,$$

where κ and ρ_f are the bulk modulus and density of air respectively, and K_s and ρ_s are the bulk modulus and density of the tissue. K_s and ρ_s are approximated by the corresponding values for water. Also, ϕ denotes the porosity, that is, the volume fraction of air.

Measurements of the speed of sound presented in [36] show good agreement with the sound speed predicted by Wood's formula for most lung volumes. However, for highly inflated lungs the measured speed of sound is higher than predicted by Woods' formula. Rice suggests that this can be due to the breakdown of the assumption of non-communication at high lung volume. A number of studies [22, 24, 27, 32] on healthy lungs inflated in the range from residual volume to total lung capacity confirm that Woods' formula gives a good prediction of the speed of sound. In [22, 27, 32] human lungs are studied and in [24] pig lungs are studied. However, in [5] Berger *et al.* study the speed of sound in lungs from fetal sheep. In this study the speed of sound is found to be considerably higher than estimated by Woods' formula and strongly frequency-dependent. It is suggested that the high speed of sound is due to greater communication between the alveoli in the fetal sheep lung than in the lungs used in the other studies.

The experimental deviations from Woods' formula in [36] and [5], and the need to interpret measurements on lung tissue with diseases such as asthma, emphysema and COPD that are associated with changes in the detailed structure of the lung at the alveolar level, motivate the development of models which include more detailed tissue mechanics. In the current work we consider the Biot equations [6, 7] as a model for the acoustic properties of lung parenchyma. The Biot equations govern small-amplitude wave propagation in a fluid-saturated porous elastic solid. The dynamic behavior of the porous material is described in terms of macroscopic, space-averaged quantities, such as acoustic pressure, elastic stress, solid and fluid displacements. The Biot model yields a frequency-dependent speed of sound.

In the Biot model, the porous material can be characterized by a number of bulk material parameters. Accurate estimation of the material parameters from measurements is difficult and in some situations (such as for biological tissues) direct measurements may be impossible. Also, some of the bulk material parameters are frequency-dependent. For the frequency-dependent parameters, only high- and low-frequency values can be obtained in measurements, and the values for intermediate frequencies are modeled, see Johnson *et al.* [18].

However, using mathematical homogenization, see *e.g.* Burridge and Keller [13] or Pride *et al.* [35], the Biot equations can be derived from a model of the micro-structure of the porous material. In the micro-structure

model the motion of the air is governed by the linearized Navier–Stokes equations and the solid frame material is governed by linear elasticity. In [13], Burridge and Keller derived two independent micro-structure problems, one so-called fluid-cell problem (a frequency-dependent flow problem governed by the unsteady Stokes equations) and one so-called solid-cell problem. The solutions of these two problems yield the bulk material parameters in the Biot equations.

Only a few papers have addressed solving fluid- and solid-cell problems for obtaining bulk material parameters. Zhou and Sheng [39] solved fluid- and solid-cell problems using a finite element method for idealized micro-structural geometries. Chapman and Higdon [14, 15] solved fluid- and solid-cell problems using a harmonic expansion technique for idealized micro-structural geometry consisting of periodic lattices of spheres in three dimensions. Terada *et al.* [38] solved fluid- and solid-cell problems in the quasi-static case using a finite element method; in [38] three-dimensional micro-scale geometries were used, involving lattices of spheres or octahedra. Burridge and Keller's approach [13] has been applied to lung parenchyma only once previously, by Owen and Lewis [31], who treated incompressible flow and considered a spatially one-dimensional unit cell.

In this paper we first introduce the Biot equations (Section 2). In Section 3, we review how homogenization can be used to derive the Biot equations following [13], and in Section 4 we demonstrate how a micro-scale simulation can be used to obtain macro-scale properties by solving a frequency-dependent fluid-cell problem numerically for an idealized two-dimensional micro-scale geometry. The main purpose of this very idealized example is to make the relation between micro-scale properties and macro-scale properties clear. In order be able to simulate macro-scale properties for parenchyma, a realistic micro-scale model should be used which takes into account the complicated micro-structure of parenchyma. In reality the parenchyma is anisotropic and inhomogeneous, but for simplicity we here consider the Biot equations for isotropic and homogeneous materials. In anisotropic, inhomogeneous cases we expect the parameters in the Biot equations to depend on direction and vary in space, respectively. In Section 5, we discuss the speed of sound for Biot materials and compare it with measured values for lung parenchyma. Finally, in Section 6 we summarize our conclusions.

2. The Biot equations

In [6, 7], Biot proposed a theory for the propagation of small-amplitude waves in a porous elastic solid saturated by a compressible viscous fluid. In [8, 9] the theory was extended and generalized. The book by Allard [1] and the paper [17] by Johnson give excellent presentations of the theory for sound propagation in porous materials including the Biot equations. In this section we give a short review of relevant parts of the Biot theory. We concentrate especially on linking the different formulations of the Biot equations that appear in the literature. First, in Section 2.1, we consider the Biot equations in the time-domain formulation, as this formulation is the easiest to physically understand, and then, in Section 2.2, we consider the Biot equations in the frequency-domain. The formulation of the Biot equations using the so-called viscodynamic operator is introduced in Section 2.3, as this formulation is the most convenient to use when discussing homogenization, as is done in Sections 3 and 4. We also, in Section 2.4, formulate the Biot equations using complex density coefficients. This formulation is used in engineering applications where parameterized approximate models have been developed for the frequency-dependent coefficients in the Biot equations. We use this in Section 5 for studying the speed of sound in Biot materials.

2.1. The Biot equations in the time-domain

Consider a system composed of a porous elastic solid frame saturated by a viscous fluid. It is assumed that the fluid is compressible and can move relative to the solid frame. It is further assumed that the pore size distribution is concentrated around its average value and that the porous material is statistically isotropic. Consider a volume of the solid-fluid system represented by a cube of unit size. Let ϕ denote the porosity, that is the volume fraction of fluid. The size of the unit element is assumed to be small compared to the wavelength of elastic waves, and the size of the unit element is assumed to be large compared to the pore size. This will give limitations for the frequencies for which the theory is valid. The relation between the alveolar size and the

sound wavelength considered below satisfies the assumptions for the relevant frequencies. Let the vector $\hat{\mathbf{U}}^s$ denote the average solid displacement and let $\hat{\mathbf{U}}^f$ denote the average fluid displacement. Based on the above assumptions, the Biot equations are formulated as

$$\rho_{11}\frac{\partial^2 \hat{\mathbf{U}}^s}{\partial t^2} + \rho_{12}\frac{\partial^2 \hat{\mathbf{U}}^f}{\partial t^2} + bF\left(\frac{\partial \hat{\mathbf{U}}^s}{\partial t} - \frac{\partial \hat{\mathbf{U}}^f}{\partial t}\right) = N\nabla^2\hat{\mathbf{U}}^s + (A+N)\nabla(\nabla \cdot \hat{\mathbf{U}}^s) + Q\nabla(\nabla \cdot \hat{\mathbf{U}}^f), \qquad (2\text{a})$$

$$\rho_{12}\frac{\partial^2 \hat{\mathbf{U}}^s}{\partial t^2} + \rho_{22}\frac{\partial^2 \hat{\mathbf{U}}^f}{\partial t^2} - bF\left(\frac{\partial \hat{\mathbf{U}}^s}{\partial t} - \frac{\partial \hat{\mathbf{U}}^f}{\partial t}\right) = Q\nabla(\nabla \cdot \hat{\mathbf{U}}^s) + R\nabla(\nabla \cdot \hat{\mathbf{U}}^f), \qquad (2\text{b})$$

compare [6, section 6] and [7, section 4]. Here, A, N, Q and R are elastic coefficients, see [6, section 2]. Their values depend on the micro-structure geometry of the porous solid, the elastic properties of the solid frame material, and the compressibility of the fluid. Also,

$$\rho_{11} = (1-\phi)\rho_s + \rho_a, \qquad (3\text{a})$$

$$\rho_{12} = -\rho_a, \qquad (3\text{b})$$

$$\rho_{22} = \phi\rho_f + \rho_a, \qquad (3\text{c})$$

where ρ_s is the density of the solid frame material, ρ_f is the density of the fluid, and ρ_a is a mass coupling parameter, the so-called added mass, see [6, section 3]. Further, $bF(\omega)$ is the frequency-dependent viscous drag coefficient, where b is related to Darcy's coefficient of permeability, k, by

$$b = \mu\phi^2/k,$$

and μ is the fluid viscosity. $F(\omega)$ is a correction factor which is introduced to correct for the frequency dependence of the viscous forces. It is normalized such that $F(0) = 1$, and we have

$$F(\omega) \sim \omega^{1/2} \quad \text{as } \omega \to \infty,$$

see [7, section 4] and [17, p 262–265].

In engineering applications, estimates of the material parameters A, N, Q, R, ρ_a, and b are typically obtained by measurements, and the correction factor $F(\omega)$ is modeled [18]. However, mathematical homogenization theory gives the tools to obtain material parameters from micro-structure simulations. In the next section, we will give a brief review of how the work by Burridge and Keller [13] can be used to obtain ρ_a, b and $F(\omega)$ by solving a fluid-cell problem, and in Section 4 we will present a numerical example for a specific idealized micro-structure geometry. The parameters A, N, Q, and R, can be obtained by solving a solid-cell problem, but we will not further consider the solid-cell problem in this paper.

Several different formulations of the Biot equations occur in the literature, and the relation between the different notations can be quite confusing. Hence, before proceeding to discussing homogenization and micro-structure simulation, we will briefly discuss some different formulations of the Biot equations, and how these formulations are related.

2.2. The Biot equations in the frequency-domain

Due to the frequency-dependent parameters in the equations, it is most convenient and common to work with the Biot equations in the frequency-domain. Assuming that all motions are time-harmonic with time dependence $e^{i\omega t}$, that is, $\hat{\mathbf{U}}^s = \mathbf{U}^s e^{i\omega t}$ and $\hat{\mathbf{U}}^f = \mathbf{U}^f e^{i\omega t}$, we obtain the frequency-domain formulation of (2),

$$-\omega^2\rho_{11}\mathbf{U}^s - \omega^2\rho_{12}\mathbf{U}^f + i\omega bF(\omega)\left(\mathbf{U}^s - \mathbf{U}^f\right) = N\nabla^2\mathbf{U}^s + (A+N)\nabla(\nabla \cdot \mathbf{U}^s) + Q\nabla(\nabla \cdot \mathbf{U}^f), \qquad (4\text{a})$$

$$-\omega^2\rho_{12}\mathbf{U}^s - \omega^2\rho_{22}\mathbf{U}^f - i\omega bF(\omega)\left(\mathbf{U}^s - \mathbf{U}^f\right) = Q\nabla(\nabla \cdot \mathbf{U}^s) + R\nabla(\nabla \cdot \mathbf{U}^f), \qquad (4\text{b})$$

compare [6, section 6] and [7, section 4].

2.3. **The Biot equations formulated using the viscodynamic operator**

The Biot theory was introduced in [6–9]. Papers [6,7] used the notation presented above, and this type of formulation of the Biot equations is most common in the literature today. However, in [8,9], a different notation was used. The homogenization results in [13] are related to the Biot equations using the formulation in [8,9], and therefore we briefly discuss how the two different formulations are related.

The Biot equations formulated using the so called viscodynamic operator is stated in [8, eq. (2.6)]. As we will only consider the fluid-cell problem, we just need to consider the equation corresponding to (4b), which in [8, eq. (2.6)] is formulated as

$$-\omega^2 \rho_f \mathbf{U}^s + i\omega \overline{Y}(\omega)\overline{\mathbf{w}} = \alpha M \nabla(\nabla \cdot \mathbf{U}^s) + M \nabla(\nabla \cdot \overline{\mathbf{w}}). \tag{5}$$

The relation between the two formulations is explained in [9]. In (5), ω, ρ_f and $\mathbf{U}^s$ are defined as above, and α, M and $\overline{\mathbf{w}}$ are related to Q, R, ϕ, $\mathbf{U}^f$ and $\mathbf{U}^s$ by

$$\overline{\mathbf{w}} = \phi(\mathbf{U}^f - \mathbf{U}^s), \tag{6a}$$

$$Q = \phi(\alpha - \phi)M, \tag{6b}$$

$$R = \phi^2 M, \tag{6c}$$

see [9, equation (2.8) and (3.31)]. By substituting (3) and (6) in (5) and comparing with (4b), we can make the identification

$$\overline{Y}(\omega) = \frac{1}{\phi^2}\left(i\omega(\phi\rho_f + \rho_a) + bF(\omega)\right). \tag{7}$$

2.4. **The Biot equations formulated using complex density coefficients**

Often (4) is formulated as

$$-\omega^2 \tilde{\rho}_{11}\mathbf{U}^s - \omega^2 \tilde{\rho}_{12}\mathbf{U}^f = N\nabla^2\mathbf{U}^s + (A+N)\nabla(\nabla \cdot \mathbf{U}^s) + Q\nabla(\nabla \cdot \mathbf{U}^f), \tag{8a}$$

$$-\omega^2 \tilde{\rho}_{12}\mathbf{U}^s - \omega^2 \tilde{\rho}_{22}\mathbf{U}^f = Q\nabla(\nabla \cdot \mathbf{U}^s) + R\nabla(\nabla \cdot \mathbf{U}^f), \tag{8b}$$

where the complex density coefficients are defined by

$$\tilde{\rho}_{11} \equiv \rho_{11} - \frac{ibF(\omega)}{\omega}, \tag{9a}$$

$$\tilde{\rho}_{12} \equiv \rho_{12} + \frac{ibF(\omega)}{\omega}, \tag{9b}$$

$$\tilde{\rho}_{22} \equiv \rho_{22} - \frac{ibF(\omega)}{\omega}. \tag{9c}$$

From (7) we find

$$\tilde{\rho}_{12} = \phi\rho_f + i\phi^2 \frac{\overline{Y}(\omega)}{\omega}$$

and one can then use the relations $\tilde{\rho}_{11} + \tilde{\rho}_{12} = (1-\phi)\rho_s$ and $\tilde{\rho}_{12} + \tilde{\rho}_{22} = \phi\rho_f$ to obtain $\tilde{\rho}_{11}$ and $\tilde{\rho}_{22}$.

In engineering applications usually the quantities static flow resistivity, σ^{static}, and tortuosity, α_∞, are used rather than b and ρ_a. These quantities are related by

$$b = \sigma^{\text{static}}\phi^2, \tag{10a}$$

$$\rho_a = \rho_f\phi(\alpha_\infty - 1). \tag{10b}$$

In [1, p. 23-24, 71-73, 127-129] the concept of static flow resistivity and tortuosity are further described and methods for measuring these quantities are discussed. Sometimes also a complex-valued so-called dynamic tortuosity $\tilde{\alpha}_\infty(\omega)$ is used, defined by

$$\tilde{\alpha}_\infty(\omega) \equiv \alpha_\infty - \frac{ibF(\omega)}{\omega\phi\rho_f}, \tag{11}$$

hence

$$\tilde{\rho}_{12} = -\left(\tilde{\alpha}_\infty(\omega) - 1\right)\rho_f\phi.$$

3. Relating the micro-scale model to the Biot parameters

Mathematical homogenization can be used to derive the Biot equations from a model of the micro-structure of the porous material, see *e.g.* Burridge and Keller [13] or Pride *et al.* [35]. In [13], two independent micro-structure problems are derived, one so-called fluid-cell problem and one so-called solid-cell problem, whose solutions yield the bulk material parameters in the Biot equations. The elastic parameters A, N, Q and R are obtained by solving the solid-cell problem, and ρ_a, b and $F(\omega)$ are obtained by solving the fluid-cell problem. Below, we will briefly review the homogenization approach used in [13]. In the next section we will present a numerical solution of a fluid-cell problem for a specific micro-structure geometry.

3.1. **The micro-scale model**

Consider again the system composed of a porous elastic solid frame saturated by a viscous fluid. Denote the solid region D_s and the fluid region D_f. Assume that h denotes a length which is characteristic for the pore size, and that H denotes a typical macroscopic length for the problem. We assume that the material is fine-grained, that is, the ratio h/H is small. We will denote this ratio by ε,

$$\varepsilon = h/H, \quad \varepsilon \ll 1.$$

We will consider motions of the fluid and solid which are small enough to be governed by the linearized Navier–Stokes equations for compressible fluids and the equations of linear elasticity respectively. The Navier–Stokes equations linearized around a background state of constant pressure and density and zero velocity are

$$\frac{\partial\tilde{p}}{\partial t} = -\kappa\nabla\cdot\tilde{\mathbf{v}}, \tag{12a}$$

$$\rho_f\frac{\partial\tilde{\mathbf{v}}}{\partial t} = \nabla\cdot\tilde{\boldsymbol{\sigma}}, \tag{12b}$$

$$\tilde{\boldsymbol{\sigma}} = -\tilde{p}I + \mu\mathsf{D}\nabla\tilde{\mathbf{v}}, \tag{12c}$$

see *e.g.* Pierce [34, section 1.5 and 10.1–2; note the use of eq. (1-5.3c)]. Here, $\tilde{p}$ denotes the pressure perturbation relative to the constant background state, $\tilde{\mathbf{v}}$ denotes the velocity, ρ_f denotes the constant background fluid density, μ denotes the fluid viscosity, and κ denotes the bulk modulus of the fluid. The linear operator D is defined such that

$$\nabla\cdot\mathsf{D}\nabla\tilde{\mathbf{v}} \equiv \nabla^2\tilde{\mathbf{v}} + \frac{1}{3}\nabla(\nabla\cdot\tilde{\mathbf{v}}).$$

The equation of motion for the solid is

$$\rho_s\frac{\partial^2\tilde{\mathbf{u}}}{\partial t^2} = \nabla\cdot\tilde{\boldsymbol{\tau}}, \tag{13}$$

where $\tilde{\mathbf{u}}$ denotes the displacement of the solid, ρ_s denotes the solid density and $\tilde{\boldsymbol{\tau}}$ is the solid stress tensor. We introduce a linear operator C that relates $\tilde{\boldsymbol{\tau}}$ to $\nabla\tilde{\mathbf{u}}$ defined such that

$$\tilde{\boldsymbol{\tau}} = E\mathsf{C}\nabla\tilde{\mathbf{u}}. \tag{14}$$

Hence C is defined by

$$\mathsf{C}\nabla\tilde{\mathbf{u}} \equiv \frac{\nu(\nabla \cdot \tilde{\mathbf{u}})}{(1+\nu)(1-2\nu)}I + \frac{\nabla\tilde{\mathbf{u}} + (\nabla\tilde{\mathbf{u}})^T}{2(1+\nu)},$$

see *e.g.* [3, pp. 12–20]. Above, E and ν denote the Young's modulus and Poisson ratio of the solid, respectively.

At the boundary $\partial D_s = \partial D_f$, we have continuity and force balance, that is,

$$\tilde{\mathbf{v}} = \frac{\partial\tilde{\mathbf{u}}}{\partial t} \quad \text{and} \quad \mathbf{n} \cdot \tilde{\boldsymbol{\sigma}} = \mathbf{n} \cdot \tilde{\boldsymbol{\tau}} \quad \text{on } \partial D_f = \partial D_s, \tag{15}$$

where $\mathbf{n}$ is the unit normal to $\partial D_f = \partial D_s$ pointing into the solid.

We now collect the equations for the fluid, (12), the equations for the solid, (13), (14), and the boundary conditions, (15). We assume that all motions are time-harmonic with time dependence $e^{i\omega t}$, that is, $\tilde{p} = pe^{i\omega t}$, $\tilde{\mathbf{v}} = \mathbf{v}e^{i\omega t}$, $\tilde{\boldsymbol{\sigma}} = \boldsymbol{\sigma}e^{i\omega t}$, $\tilde{\mathbf{u}} = \mathbf{u}e^{i\omega t}$, and $\tilde{\boldsymbol{\tau}} = \boldsymbol{\tau}e^{i\omega t}$, and arrive at the micro-scale model

$$i\omega\rho_f\mathbf{v} = \nabla \cdot \boldsymbol{\sigma}, \qquad \text{in } D_f, \tag{16a}$$
$$\boldsymbol{\sigma} = -pI + \mu\mathsf{D}\nabla\mathbf{v}, \quad \text{in } D_f, \tag{16b}$$
$$i\omega p = -\kappa\nabla \cdot \mathbf{v}, \qquad \text{in } D_f, \tag{16c}$$
$$\mathbf{v} = i\omega\mathbf{u}, \qquad \text{on } \partial D_f = \partial D_s, \tag{16d}$$
$$\mathbf{n} \cdot \boldsymbol{\sigma} = \mathbf{n} \cdot \boldsymbol{\tau}, \qquad \text{on } \partial D_f = \partial D_s, \tag{16e}$$
$$-\omega^2\rho_s\mathbf{u} = \nabla \cdot \boldsymbol{\tau}, \qquad \text{in } D_s, \tag{16f}$$
$$\boldsymbol{\tau} = \mathsf{C}\nabla\mathbf{u}, \qquad \text{in } D_s. \tag{16g}$$

3.2. The homogenization method

In [13], the two-scale method of homogenization, [4, 19, 37], is used to derive equations governing the gradual variation of space-averaged quantities such as acoustic pressure, elastic stress, solid and fluid displacements from the micro-scale model (16). The average is taken over the micro-scale variations. In the method, it is assumed that for all properties of the porous system, that is, $\mathbf{v}$, $\boldsymbol{\sigma}$, p, $\mathbf{u}$, and $\boldsymbol{\tau}$, the variations at the micro-scale and macro-scale can be separated. This is done by expressing the space dependence of the solid displacement in the form

$$\mathbf{u} = \mathbf{u}(\mathbf{x}, \mathbf{y})$$

and similarly for the other variables. Here $\mathbf{x}$ is the ordinary position vector, and $\mathbf{y}$ is the position vector in a stretched coordinate system

$$\mathbf{y} = \varepsilon^{-1}\mathbf{x}.$$

Hence, the first argument in $\mathbf{u}(\mathbf{x}, \mathbf{y})$ accounts for the slow macro-scale variations, and the second argument accounts for the rapid micro-scale variations. Here we assume that the micro-scale variations are periodic functions of $\mathbf{y}$, that is, the macro-structure is obtained by repeating a specific block of micro-structure. In tissue, there are random variations in the micro-structure. The same homogenization method can be used when there are random variations in the micro-structure, see [13], but the evaluation of the fluid- and solid-cell problems will be more complicated. However, the most important concepts are captured without considering random variations at the micro-scale.

It is further assumed that the two sets of variables $\mathbf{x}$ and $\mathbf{y}$ are independent, and that derivatives can be separated into one macro-scale component and one micro-scale component,

$$\nabla\mathbf{u} = \nabla_{\mathbf{x}}\mathbf{u} + \varepsilon^{-1}\nabla_{\mathbf{y}}\mathbf{u}.$$

It is also assumed that each property of the porous material can be expanded in an asymptotic power series in ε, that is,

$$\mathbf{u}(\mathbf{x}, \mathbf{y}, \varepsilon) = \mathbf{u}_0(\mathbf{x}, \mathbf{y}) + \varepsilon\mathbf{u}_1(\mathbf{x}, \mathbf{y}) + \varepsilon^2\mathbf{u}_2(\mathbf{x}, \mathbf{y}) + \mathcal{O}(\varepsilon^3). \tag{17}$$

The Biot equations were formulated in [6, 7] to capture the large scale behavior for frequencies ranging from low frequencies, where the character of the micro-scale flow is dominated by viscous effects (Poiseuille flow), to high frequencies, where the micro-scale flow is dominated by inertial effects. Depending on what assumption that is made on the Reynolds number in the homogenization process, different large scale equations will be obtained. In order to obtain the Biot equations, one formally assumes that the Reynolds number appropriate for the micro-scale flow, $h^2\omega\rho_f/\mu = \tilde{\mu}^{-1}$, say is of order unity, for details see [13]. This is a distinguished limit in which viscous and inertial effects are in balance, and it readily allows the limits $\tilde{\mu}^{-1} \ll 1$ and $\tilde{\mu}^{-1} \gg 1$ subsequently to be investigated.

By substituting all these assumptions in (16) and matching terms multiplying the same power of ε, a number of relations are obtained. These relations correspond to the behavior of the system in the limit when $\varepsilon \to 0$. By applying an averaging procedure to some of these relations (in order to average out the $\mathbf{y}$ dependence) the Biot equations are obtained.

3.3. The fluid-cell problem

The viscodynamic operator $\overline{Y}(\omega)$, see (7), and thereby the parameters ρ_a, b and $F(\omega)$, are related to the space average over the micro-structure of the displacement of fluid relative to solid, see (5) and (6a). The fluid-cell problem is a flow problem at the micro-scale which can be used to compute $\overline{Y}(\omega)$.

Let us first define $\mathbf{w}(\mathbf{x}, \mathbf{y})$, the displacement of the fluid relative to the solid (at the micro-scale), by

$$\mathbf{v}_0(\mathbf{x}, \mathbf{y}) = i\omega\left(\mathbf{u}_0(\mathbf{x}) + \mathbf{w}(\mathbf{x}, \mathbf{y})\right),$$

where $\mathbf{v}_0$ and $\mathbf{u}_0$ are the first-order terms in the expansions of the fluid velocity and solid displacement respectively, see (17). In the homogenization procedure a set of equations for $\mathbf{w}$ is obtained. It is formulated as the unsteady Stokes equation for $\mathbf{w}$ to be solved on a unit cube in the micro-scale,

$$-\omega^2\rho_f\mathbf{w}(\mathbf{x}, \mathbf{y}) - i\omega\hat{\mu}\nabla_{\mathbf{y}}^2\mathbf{w}(\mathbf{x}, \mathbf{y}) + \nabla_{\mathbf{y}}p_1(\mathbf{x}, \mathbf{y}) = \nabla_{\mathbf{x}} \cdot \boldsymbol{\sigma}_0(\mathbf{x}) + \omega^2\rho_f\mathbf{u}_0(\mathbf{x}), \quad \text{in } D_f, \tag{18a}$$

$$\nabla_{\mathbf{y}} \cdot \mathbf{w}(\mathbf{x}, \mathbf{y}) = 0, \qquad\qquad\qquad \text{in } D_f, \tag{18b}$$

$$\mathbf{w}(\mathbf{x}, \mathbf{y}) = 0, \qquad\qquad\qquad \text{on } \partial D_f = \partial D_s, \tag{18c}$$

with the additional boundary condition that there should be periodicity across the unit cube, compare [13, eq. (13)-(15), note the sign error in (15a)]. Here, $\boldsymbol{\sigma}_0$ is the first-order term in the expansion of the fluid stress tensor, and p_1 is the $\mathcal{O}(\varepsilon)$ term in the expansion of the fluid pressure. Also, $\hat{\mu} = \mu H^2/h^2$. Note that the right-hand side of (18) is independent of $\mathbf{y}$ while the left-hand side of (18) depends both on $\mathbf{x}$ and $\mathbf{y}$. As $\mathbf{y}$ accounts for variations on the rapidly varying micro-scale, and $\mathbf{x}$ accounts for variations on the slowly varying macro-scale, and these two scales are assumed to be separated, the right-hand side can be regarded as a uniform forcing when (18) is solved.

Since (18) is linear in $\mathbf{w}$, the solution can be expressed as

$$\mathbf{w}(\mathbf{x}, \mathbf{y}, \omega) = W(\mathbf{x}, \mathbf{y}, \omega)\left(\nabla_{\mathbf{x}} \cdot \boldsymbol{\sigma}_0(\mathbf{x}) + \omega^2\rho_f\mathbf{u}_0(\mathbf{x})\right), \tag{19}$$

where $W(\mathbf{x}, \mathbf{y}, \omega)$ is a matrix. W_{ij} can be obtained by solving (18) with the right-hand side term $\nabla_{\mathbf{x}} \cdot \boldsymbol{\sigma}_0(\mathbf{x}) + \omega^2\rho_f\mathbf{u}_0(\mathbf{x})$ replaced by a unit vector in the $\mathbf{y}_j$ direction.

We now take the space average of (19) and obtain

$$\overline{\mathbf{w}}(\mathbf{x}, \omega) = \overline{W}(\omega)\left(\nabla_{\mathbf{x}} \cdot \boldsymbol{\sigma}_0(\mathbf{x}) + \omega^2\rho_f\mathbf{u}_0(\mathbf{x})\right). \tag{20}$$

Here, we have restricted our interest to macroscopically uniform media, that is assuming that the average $\overline{W}$ is independent of $\mathbf{x}$. Under the assumption that the matrix $\overline{W}(\omega)$ is invertible, we can now rewrite (20) as

$$-\omega^2\rho_f\mathbf{u}_0(\mathbf{x}) + [\overline{W}(\omega)]^{-1}\overline{\mathbf{w}}(\mathbf{x}) = \nabla_{\mathbf{x}} \cdot \boldsymbol{\sigma}_0(\mathbf{x}). \tag{21}$$
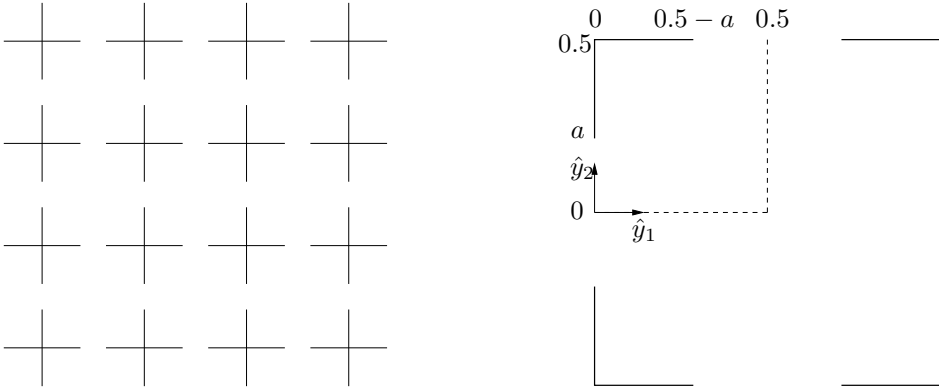
FIGURE 1. Left; A 2D idealized micro-scale geometry. Each micro-scale cell is square. The cells are separated by infinitely thin walls, and are connected by an opening in the middle of each of the walls. Right; The geometry of a single cell. The sides of the cell are of unit length in the $(\hat{y}_1, \hat{y}_2)$-coordinate system. Centered around the middle of each wall is an opening of width $2a$. The dashed lines indicate lines of symmetry.

Equation (21) corresponds to (5) and we can make the identifications $\mathbf{u}_0 = \mathbf{U}^s$ and

$$[\overline{W}(\omega)]^{-1} = i\omega\overline{Y}(\omega).$$

The term $\nabla_{\mathbf{x}} \cdot \boldsymbol{\sigma}_0(\mathbf{x})$ can be identified with the right-hand side of (5). However, this is more involved and for details we refer to [13].

4. NUMERICAL SOLUTION OF A FLUID-CELL PROBLEM

We now consider a two-dimensional idealized micro-scale geometry, as illustrated in Figure 1. Each micro-scale cell is assumed to be square, with sides having physical length h. The cells are separated by infinitely thin walls, and are connected to each other by an opening in the middle of each wall. Our goal in this section is to compute the viscodynamic operator $\overline{Y}(\omega)$ corresponding to this geometry.

4.1. Non-dimensionalization

In order to make the parameter dependence clear, we non-dimensionalize (18) by introducing dimensionless variables

$$\hat{\mathbf{x}} = \frac{\mathbf{x}}{H}, \quad \hat{\mathbf{y}} = \frac{\mathbf{y}}{H}, \quad \hat{\mathbf{w}} = \frac{\mathbf{w}}{\delta}, \quad \overline{\hat{\mathbf{w}}} = \frac{\overline{\mathbf{w}}}{\delta}, \quad \hat{\mathbf{u}}_0 = \frac{\mathbf{u}_0}{\delta}, \quad \hat{p}_1 = \frac{p_1 H}{\kappa\delta}, \quad \hat{\boldsymbol{\sigma}}_0 = \frac{\boldsymbol{\sigma}_0 H}{\kappa\delta}, \quad \hat{\rho} = \frac{\rho_f}{\rho_s},$$

where δ is a length characteristic of the amplitude of fluid and solid displacements. The length H is related to κ, ω and ρ_s by

$$H^2 = \frac{\kappa}{\rho_s\omega^2},$$

that is, H corresponds to the wavelength of waves balancing fluid compressibility with solid inertia. The scaling for $\hat{\mathbf{y}}$ is chosen such that $|\hat{\mathbf{y}}| = 1$ at $|\mathbf{x}| = h$, hence, a micro-cell is of unit length in the $\hat{\mathbf{y}}$ coordinate system. In

the rescaled variables, equation (18) can be expressed as

$$-\hat{\mathbf{w}} - i\tilde{\mu}\nabla_{\hat{\mathbf{y}}}^2\hat{\mathbf{w}} + \frac{1}{\hat{\rho}}\nabla_{\hat{\mathbf{y}}}\hat{p}_1 = \frac{1}{\hat{\rho}}\nabla_{\hat{x}} \cdot \boldsymbol{\sigma}_0 + \hat{\mathbf{u}}_0, \quad \text{in } D_f, \tag{22a}$$

$$\nabla_{\hat{\mathbf{y}}} \cdot \hat{\mathbf{w}} = 0, \qquad\qquad \text{in } D_f, \tag{22b}$$

$$\hat{\mathbf{w}} = 0, \qquad\qquad \text{on } \partial D_f, \tag{22c}$$

and in addition we have periodicity, that is $\hat{\mathbf{w}}(\hat{y}_1 + 1, \hat{y}_2) = \hat{\mathbf{w}}(\hat{y}_1, \hat{y}_2)$ and $\hat{\mathbf{w}}(\hat{y}_1, \hat{y}_2 + 1) = \hat{\mathbf{w}}(\hat{y}_1, \hat{y}_2)$. Also

$$\tilde{\mu} \equiv \frac{\mu}{h^2\omega\rho_f}$$

is an inverse Reynolds number that is formally assumed to be of order unity.

In the transformed variables, the equation corresponding to (20) is

$$\overline{\hat{\mathbf{w}}} = \overline{\hat{W}}(\omega)\left(\frac{1}{\hat{\rho}}\nabla_{\hat{\mathbf{x}}} \cdot \boldsymbol{\sigma}_0 + \hat{\mathbf{u}}_0\right). \tag{23}$$

After transforming back to original variables and rearranging we obtain

$$-\omega^2\rho_f\mathbf{u}_0(\mathbf{x}) + \rho_f\omega^2[\overline{\hat{W}}(\omega)]^{-1}\overline{\mathbf{w}}(\mathbf{x}) = \nabla_{\mathbf{x}} \cdot \boldsymbol{\sigma}_0(\mathbf{x}),$$

which corresponds to (21). Hence

$$\overline{Y}(\omega) = -i\rho_f\omega[\overline{\hat{W}}(\omega)]^{-1}.$$

4.2. Numerical solution

The fluid cell problem (22) with the right-hand side replaced by the unit vector $\mathbf{F} = (1,0)^T$ was solved using complex $P_2 - P_1$ Taylor–Hood[1] finite elements, that is, the velocity was discretized using (complex) piecewise quadratic polynomials and the pressure was discretized using (complex) piecewise linear polynomials. The solution was computed on a 128×128 triangular mesh (resulting in a system with 297,478 unknowns) using DOLFIN/FFC [20, 21, 25, 26]. The parameter values $\mu = 1.7 \cdot 10^{-5}\text{Pa}\,\text{s}$, $\rho_s = 10^3\text{kg/m}^3$, $h = 10^{-4}\text{m}$, $\rho_f = 1.3\text{kg/m}^3$ were used. The solution $\hat{\mathbf{w}}(\hat{y}_1, \hat{y}_2, \omega)$ was computed for a wide range of frequencies, $\omega \in (10\text{s}^{-1}, 10^7\text{s}^{-1})$, corresponding to an inverse Reynolds number $\tilde{\mu}$ ranging from $\frac{1.7}{1.3} \times (10^{-4} - 10^2)$ and a density ratio $\hat{\rho} = 1.3 \times 10^{-3}$. For low frequencies, the flow is smooth and viscous, while for higher frequencies the viscous effects decrease, see Figures 2 and 3.

The average $\overline{\hat{\mathbf{w}}}(\omega)$ is defined as the integral of $\hat{\mathbf{w}}(\hat{y}_1, \hat{y}_2, \omega)$ over the fluid region of the unit cube multiplied by the volume fraction of fluid in the unit cube, see [13]. As the solid walls for the current geometry are infinitely thin, we arrive at

$$\overline{\hat{\mathbf{w}}}(\omega) = \begin{pmatrix} \overline{\hat{w}}_1(\omega) \\ \overline{\hat{w}}_2(\omega) \end{pmatrix} = \int_{\hat{y}_2=-0.5}^{\hat{y}_2=0.5}\int_{\hat{y}_1=0}^{\hat{y}_1=1} \hat{\mathbf{w}}(\hat{y}_1, \hat{y}_2, \omega)d\hat{y}_1 d\hat{y}_2. \tag{24}$$

Due to the symmetry of the flow, we have $\overline{\hat{w}}_2(\omega) = 0$.

Two entries in the matrix $\overline{\hat{W}}(\omega)$ can now be computed using the relation (23) (recall that the right-hand side has been replaced by the unit vector $\mathbf{F} = (1,0)^T$). We obtain

$$\overline{\hat{W}}_{11} = \overline{\hat{w}}_1(\omega), \quad \overline{\hat{W}}_{21} = 0.$$

---

[1]The Taylor–Hood element is a standard finite element that fulfills the Babuška–Brezzi condition necessary for convergence (see [2, 11, 12]).

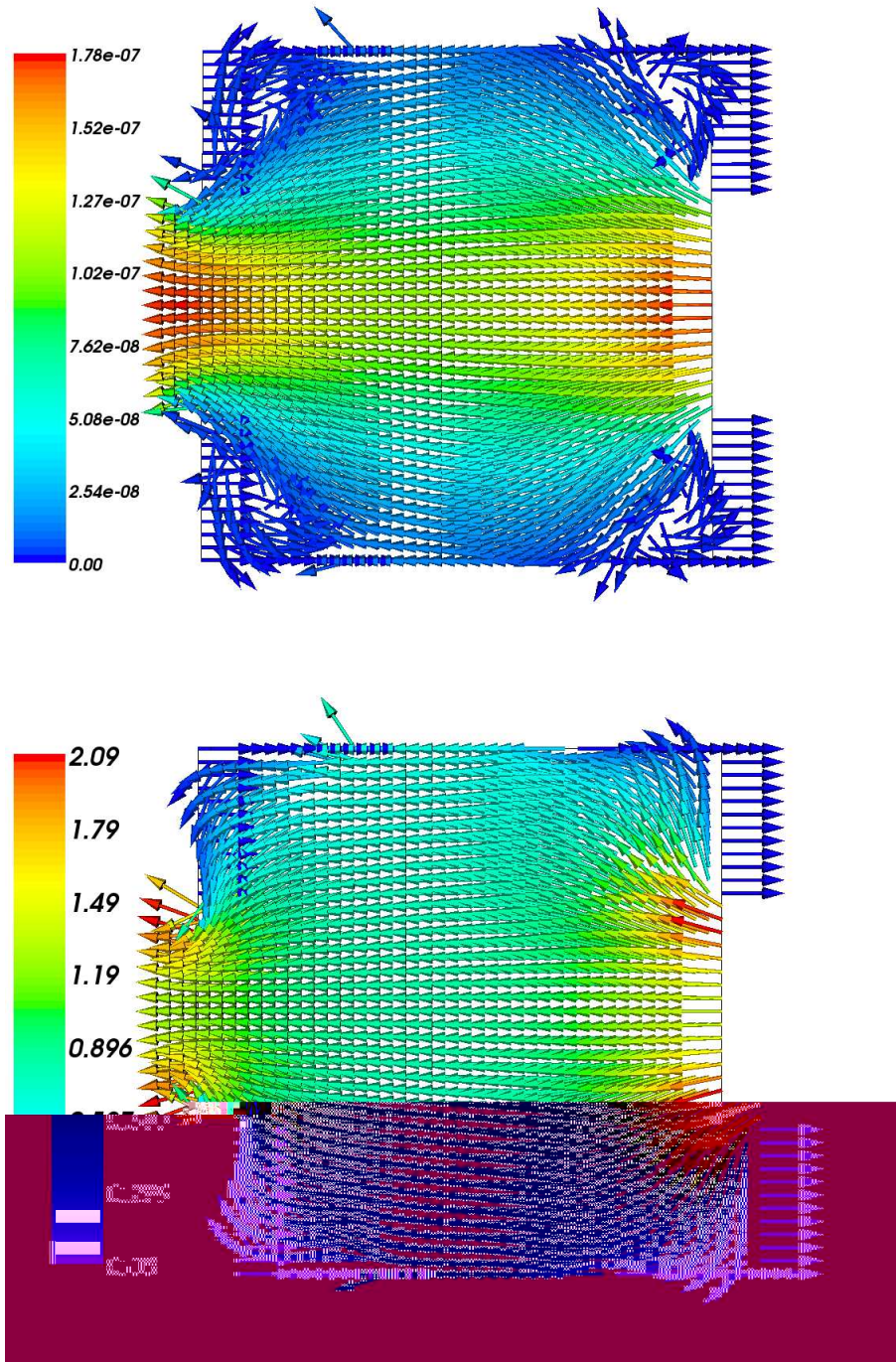FIGURE 2. Above, the real part of $\hat{\mathbf{w}}$ is plotted for $\omega = 10\mathrm{s}^{-1}$ (top) and $\omega = 10^6\mathrm{s}^{-1}$ (bottom). This quantity corresponds to the instantaneous displacement field at $t = 0$. In both cases, $a = 0.2$. The above plots were obtained on a 40×40 triangular mesh (a finer 128×128 triangular mesh was used when computing $\overline{Y}(\omega)$). The rightward pointing arrows along parts of the cell boundary is due to the plotting program placing arrows directed along the positive $\hat{y}_1$ axis for zero-valued points.
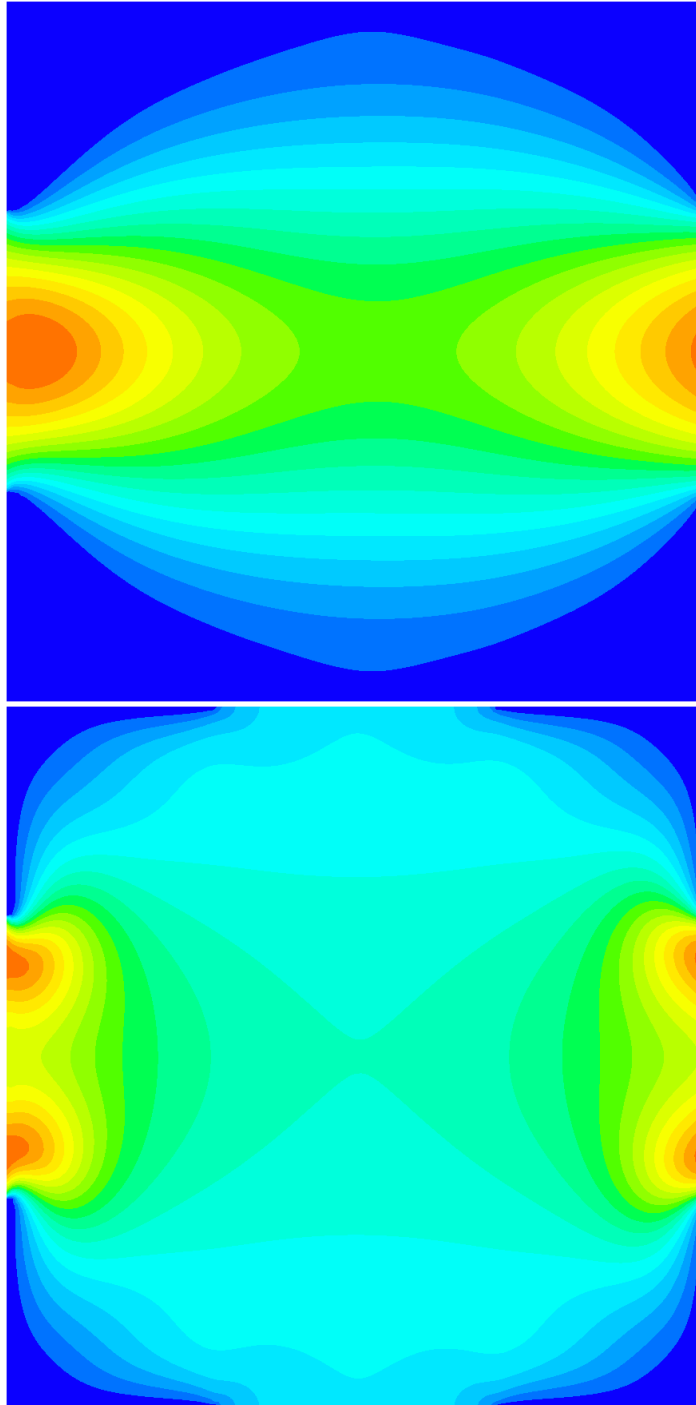
FIGURE 3. To further clarify the difference in the character of the displacement field in the low- and high-frequency range, we above plot the norm of the real part of $\hat{\mathbf{w}}$ for $\omega = 10\text{s}^{-1}$ (top) and $\omega = 10^6\text{s}^{-1}$ (bottom). In both cases, $a = 0.2$, and the plots were obtained on a 128×128 triangular mesh.

The remaining two entries can be computed by solving the fluid-cell problem with the right-hand replaced by the unit vector $\mathbf{G} = (0,1)^T$. However, due to the symmetry of the geometry we find

$$\overline{\hat{W}}_{12} = 0, \quad \overline{\hat{W}}_{22} = \overline{\hat{w}}_1(\omega),$$

and we arrive at

$$\overline{\hat{W}}(\omega) = \overline{\hat{w}}_1(\omega)I,$$

where I is the identity matrix. Hence, in this case the viscodynamic operator $\overline{Y}(\omega)$ is a scalar,

$$\overline{Y}(\omega) = -i\rho_f\omega\overline{\hat{w}}_1^{-1}(\omega). \tag{25}$$

Using (24) and (25), we can compute $\overline{Y}(\omega)$. In Figure 4, the modulus and the phase of $\overline{Y}(\omega)$ are plotted as a function of ω for different values of a, the size of the openings between the cells. In order to verify that the computed solutions have the right asymptotic behavior, we consider a large range of frequencies. As expected from (7), $\overline{Y}(\omega)$ asymptotes towards a real, positive value as $\omega \to 0$, and for large values of ω, $\overline{Y}(\omega)$ is linear in ω with a purely imaginary constant of proportionality. The latter limit captures the added mass term $\phi\rho_f + \rho_a$ in (7) which is dominant at high frequencies. At high frequencies, viscous effects are confined to boundary layers at the edge of the cell of width $(\mu/\omega\rho_f)^{1/2} \ll h$. These contribute to the $\mathcal{O}(\omega^{1/2})$ viscous correction F in (7).

5. Speed of sound

In this section we will first derive an expression for the speed of sound in Biot materials, in terms of the bulk material parameters discussed in Section 2. We will then specifically study the speed of sound in the parameter ranges valid for lung parenchyma. We find that due to the characteristics of the parenchyma, it is relatively easy to obtain estimates of the elastic parameters A, N, Q and R (which however also can be obtained by solving the solid-cell problem). We then discuss how the speed of sound depends on the parameters related to fluid motion in the porous material, ρ_a, b and $F(\omega)$ (which via the viscodynamic operator $\overline{Y}(\omega)$ can be obtained by solving the fluid-cell problem), and use parameter fitting to show that the Biot model yields a frequency dependence of the speed of sound which is in qualitative agreement with the measurements in [5]. From a micro-structure problem it is straightforward to obtain the frequency dependence of the speed of sound for that specific micro-scale geometry. However, by using a parameterized bulk model (the Johnson model, see (34) below, which gives an approximation of the frequency dependence), it is possible to study the bulk material behavior for whole parameter ranges, making it easier to understand what different types of behavior can be expected.

5.1. **Speed of sound for Biot materials**

Three different kinds of waves can propagate in a Biot material, two compression waves and one shear wave, see [6]. The two compression waves are denoted the slow and the fast wave respectively. The fast compression wave corresponds to sound propagation. In order to obtain the wave propagation speeds for the compression waves, we follow [6] and apply the divergence operation to (8). We obtain

$$-\omega^2 \left(\tilde{\rho}_{11}e + \tilde{\rho}_{12}\epsilon \right) = \nabla^2 \left(Pe + Q\epsilon \right), \tag{26a}$$

$$-\omega^2 \left(\tilde{\rho}_{12}e + \tilde{\rho}_{22}\epsilon \right) = \nabla^2 \left(Qe + R\epsilon \right), \tag{26b}$$

where $e = \nabla \cdot \mathbf{U}^s$, $\epsilon = \nabla \cdot \mathbf{U}^f$ and $P = A + 2N$. We make the ansatz

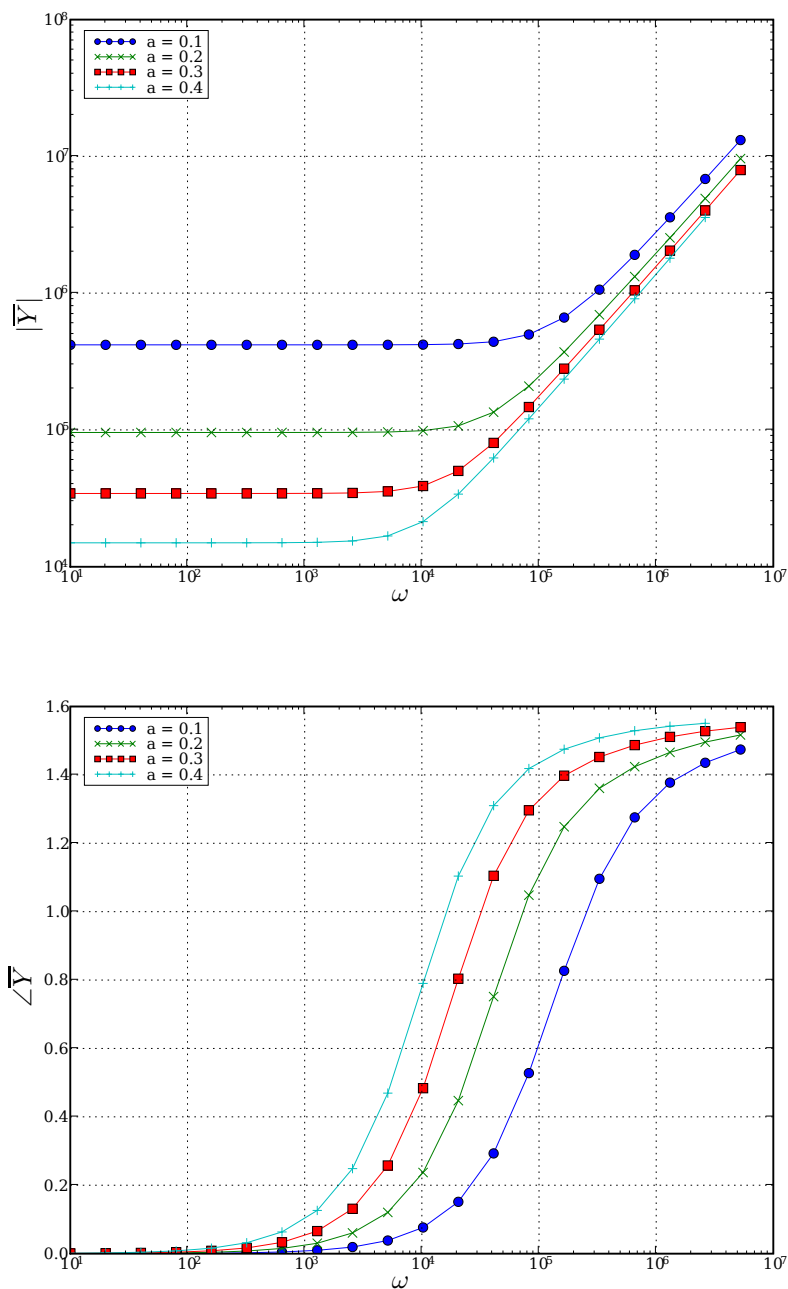$$e = C_1 e^{iqx}, \tag{27a}$$

$$\epsilon = C_2 e^{iqx}. \tag{27b}$$

FIGURE 4. Modulus (top) and phase (bottom) of the viscodynamic operator $\overline{Y}$ as function of the frequency ω for different values of $a = 0.1, 0.2, 0.3, 0.4$.

The wave speed of these waves is

$$V = \omega/q.$$

Substituting (27) into (26) gives

$$\begin{pmatrix} P - z\tilde{\rho}_{11} & Q - z\tilde{\rho}_{12} \\ Q - z\tilde{\rho}_{12} & R - z\tilde{\rho}_{22} \end{pmatrix} \begin{pmatrix} C_1 \\ C_2 \end{pmatrix} = 0, \tag{28}$$

where $z = V^2$. Equation (28) has a non-trivial solution only if the matrix determinant is equal to zero. This gives a quadratic equation for z,

$$(\tilde{\rho}_{11}\tilde{\rho}_{22} - \tilde{\rho}_{12}^2)z^2 - (P\tilde{\rho}_{22} + R\tilde{\rho}_{11} - 2Q\tilde{\rho}_{12})z + (PR - Q^2) = 0. \tag{29}$$

Solving (29) yields

$$V_{\text{fast,slow}}^2 = \frac{\Delta \pm \sqrt{\Delta^2 - 4(\tilde{\rho}_{11}\tilde{\rho}_{22} - \tilde{\rho}_{12}^2)(PR - Q^2)}}{2(\tilde{\rho}_{11}\tilde{\rho}_{22} - \tilde{\rho}_{12}^2)}, \tag{30}$$

where the positive sign gives the wave propagation speed of the fast wave and

$$\Delta \equiv P\tilde{\rho}_{22} + R\tilde{\rho}_{11} - 2Q\tilde{\rho}_{12}.$$

5.2. **Parameter ranges valid for lung parenchyma**

From a number of so-called gedanken experiments, Biot derived expressions for the elastic constants P, Q and R as functions of ϕ, κ, K_s, K_b and N,

$$P = \frac{(1 - \phi)(1 - \phi - K_b/K_s)K_s + \phi K_s K_b/\kappa}{1 - \phi - K_b/K_s + \phi K_s/\kappa} + \frac{4}{3}N, \tag{31a}$$

$$Q = \frac{(1 - \phi - K_b/K_s)\phi K_s}{1 - \phi - K_b/K_s + \phi K_s/\kappa}, \tag{31b}$$

$$R = \frac{\phi^2 K_s}{1 - \phi - K_b/K_s + \phi K_s/\kappa}, \tag{31c}$$

see [10] or [1, p. 118-122]. Here K_b is the bulk modulus of the solid frame at constant fluid pressure, and N is the shear modulus of the frame. As approximations for K_b and N we use measured values of the bulk modulus and shear modulus for human lungs, see Lai-Fook and Hyatt [23] where it is investigated how these values vary with lung volume and age. We use $K_b = 10^4$ Pa and $N = 10^3$ Pa.

In the parenchyma, we have a porous solid with gas-filled pores. Since a solid is much stiffer than a gas, that is, $K_s \gg \kappa$, and parenchyma is a material with a weak frame, that is, $K_b, N \ll \kappa, K_s$, the expressions for P, Q, R may be simplified to

$$P = K_b + \frac{(1 - \phi)^2}{\phi}\kappa + \frac{4}{3}N, \tag{32a}$$

$$Q = (1 - \phi)\kappa, \tag{32b}$$

$$R = \phi\kappa, \tag{32c}$$

see [1, p. 122-124].

We will now discuss the relation between the speed of sound for a Biot material (30) and the speed of sound predicted by Woods' formula (1), for details see [17]. In the limit $|\tilde{\alpha}_\infty(\omega)| \to \infty$, it is straightforward to show that the expression for the wave speed of the fast wave, (30), simplifies to

$$V_{\text{fast}}^2 = \frac{H}{(1 - \phi)\rho_s + \phi\rho_f}, \tag{33}$$

where

$$H = P + 2Q + R = \frac{K_s + (\phi K_s/\kappa - (1 + \phi)) K_b}{1 - \phi - K_b/K_s + \phi K_s/\kappa} + \frac{4}{3}N.$$

Note that (33) is independent of frequency. From the definition of $\tilde{\alpha}_\infty(\omega)$ in (11), it can be seen that a large value of $|\tilde{\alpha}_\infty(\omega)|$ is characteristic of situations where the fluid motion relative to the solid is very restricted, as in the low frequency limit, $\omega \to 0$, and also if the viscous drag coefficient b is large. In these two cases, the relative motion is restricted by large viscous forces. The fluid can also be locked to the solid by a large inertial effect, that is a high tortuosity α_∞.

As mentioned above, parenchyma is a material with a weak frame, that is

$$K_b, N \ll \kappa, K_s.$$

In this limit, the speed of sound V_{fast} given by (33) asymptotes towards Wood's formula, (1). Expressions for the deviation from Wood's formula are given in [17, p. 271].

To summarize, for a material with a weak frame, the speed of sound is always close to the value predicted by Wood's formula in the low frequency limit. If the fluid motion relative to the solid is very restricted (as *e.g.* in the model with non-communicating air bubbles, [36]) the speed of sound will be constant, independent of frequency. Otherwise the speed of sound will be frequency dependent.

We now use equation (30) to demonstrate how the speed of sound varies depending on the parameters σ^{static} and α_∞. We use (32) for P, Q and R, and approximate the correction factor $F(\omega)$ using the Johnson model,

$$F(\omega) = \sqrt{1 - i\omega \frac{4\mu\rho_f\alpha_\infty^2}{\phi^2(\sigma^{\text{static}})^2\Lambda^2}}, \tag{34}$$

see Johnson *et al.* [18] or *e.g.* Göransson [16] and references therein for an exhaustive discussion of this model. Here, Λ is the so-called viscous characteristic length, a parameter introduced in [18].

In Figure 5, the speed of sound is plotted for various combinations of values of σ^{static} and α_∞. The remaining
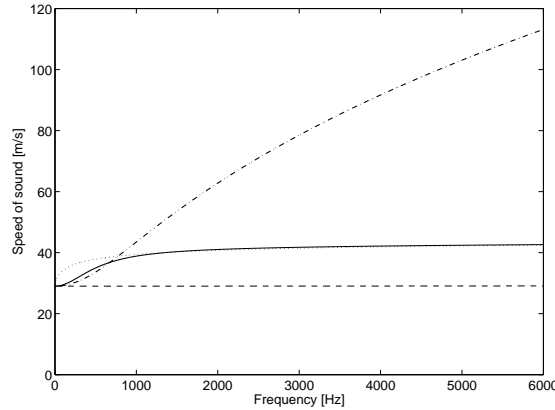

FIGURE 5. Speed of sound as function of frequency in Biot materials for some different values of static flow resistivity and tortuosity; $\sigma^{\text{static}} = 10^6\text{kg/m}^3\text{s}$, $\alpha_\infty = 100$ (solid line), $\sigma^{\text{static}} = 10^8\text{kg/m}^3\text{s}$, $\alpha_\infty = 1.2$ (dashed line), $\sigma^{\text{static}} = 10^6\text{kg/m}^3\text{s}$, $\alpha_\infty = 1.2$ (dash-dotted line), $\sigma^{\text{static}} = 10^4\text{kg/m}^3\text{s}$, $\alpha_\infty = 100$ (dotted line). In all cases $\mu = 1.7 \cdot 10^{-5}\text{Pa s}$, $\rho_f = 1.3\text{kg/m}^3$, $\kappa = 1.5 \cdot 10^5\text{Pa}$, $\phi = 0.75$ and $\Lambda = 1.25 \cdot 10^{-4}\text{m}$.

parameters have been chosen as follows. As in the fluid cell problem we have used $\mu = 1.7 \cdot 10^{-5}\text{Pa s}$ and

Volume of air [ml]	Speed of sound [m/s]	
	500 Hz	5000 Hz
40	33.6	68.5
60	29.8	63.0
80	27.7	57.4
120	27.7	51.5
180	25.5	47.7
240	27.7	42.1

TABLE 1. Data obtained from [5, Figure 5].

$\rho_f = 1.3$kg/m^3. For the bulk modulus of air $\kappa = 1.5 \cdot 10^5$Pa was used (note that no value for K_s was needed as the simplified expression (32) was used for P, Q and R). The volume fraction of air in the parenchyma ϕ was chosen in the middle of the physiological range to be $\phi = 0.75$, see [36]. Information on Λ for parenchyma was not available, therefore we have here used a typical value for polymer foam, $\Lambda = 1.25 \cdot 10^{-4}$m. As expected from the discussion above, the speed of sound in the low frequency limit $\omega \to 0$ asymptotes towards Wood's formula, independent of the values of σ^{static} and α_∞. As the frequency increases, the speed of sound increases, and the exact form of the graph depends on the values of σ^{static} and α_∞. We note that in the example with a very high value for the static flow resistivity, $\sigma^{\text{static}} = 10^8$kg/m^{3}s, the speed of sound stays very close to Wood's formula for all the frequencies displayed in Figure 5. This behavior is in agreement with the experimental results presented in [22, 24, 27, 32, 36].

In measurements presented in [5], the speed of sound through lungs of fetal sheep was found to be much higher than predicted by Wood's formula. Also, the speed of sound was strongly frequency-dependent. Qualitative agreement with these findings can be obtained using the Biot model. In [5], lungs from fetal sheep were excised without allowing air to enter the liquid-filled lungs. After withdrawing fetal liquid from the lungs, the lungs had an average weight of 151.4 g. Air was then injected in the lungs, and the frequency dependence of the speed of sound was measured with the lungs filled with 40, 60, 80, 120, 180 and 240 ml of air respectively. The tissue density was assumed to be 1 g/ml. The results of these measurements are presented in [5, Figure 5]. By measurements in that figure, we obtained values for the measured values of speed of sound at 500 Hz and 5000 Hz, see Table 1. The porosity of the lungs can be computed from the information about lung weight and volume of air in the lungs. The parameters σ^{static}, α_∞, Λ were fitted to the measured values using one iteration of the Gauss-Newton method from the starting guess $\sigma^{\text{static}} = 4 \cdot 10^6$kg/m^{3}s, $\alpha_\infty = 23$, $\Lambda = 1.25 \cdot 10^{-4}$m, arriving at the values $\sigma^{\text{static}} = 5.25 \cdot 10^6$kg/m^{3}s, $\alpha_\infty = 26.5$, $\Lambda = 4.02 \cdot 10^{-4}$m. In Figure 6, the speed of sound for the fitted parameter values are plotted. The sound speed increases with frequency but falls with lung inflation.

6. CONCLUSIONS

Current modeling of the acoustic properties of the parenchyma is based on the assumption that the air motion between the alveoli is negligible [36]. The parenchyma is considered as a homogeneous mixture of air and lung tissue, and the speed of sound can then be computed from the average parenchyma density and the average bulk modulus of the mixture. The speed of sound is independent of frequency and is given by the so-called Wood's formula (1). The predicted speed of sound has been confirmed in several experimental studies on human lungs in volume ranges from residual volume to total lung capacity [22, 24, 27, 32]. However, for high lung volumes the measured speed of sound in horse lungs is considerably higher than predicted by this theory [36]. Also, in a recent study on lungs from fetal sheep, the measured speed of sound is considerably higher than predicted by Wood's formula and also strongly frequency-dependent [5]. In [36] it is suggested that the deviation from Wood's formula is due to increasing communication between alveoli as lung volume increases, and in [5] it is suggested that fetal sheep might have a relatively open alveoli structure.
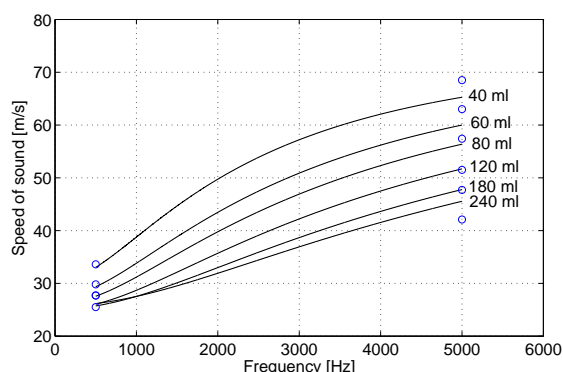
FIGURE 6. Speed of sound for varying porosity corresponding to the measurements in [5]. The fitted parameter values $\sigma^{\text{static}} = 5.25 \cdot 10^6 \text{kg/m}^3\text{s}$, $\alpha_\infty = 26.5$, $\Lambda = 4.02 \cdot 10^{-4}\text{m}$ are used. Circles correspond to measurements at 500Hz and 5000Hz, see Table 1.

In this paper we consider the Biot equations as a model for the acoustic properties of lung parenchyma. In the Biot model, effects of motion of fluid relative to the porous solid frame are included. We have reviewed how homogenization can be used to derive the Biot equations from a model of the micro-structure of a porous material. The bulk material parameters in the Biot equations related to the motion of fluid relative to solid can be obtained by solving a flow problem at the micro-scale, the fluid-cell problem. We have solved a fluid-cell problem numerically for an idealized micro-structure geometry for a wide range of frequencies.

The speed of sound in a Biot material is highly dependent on the micro-structure. Parenchyma is a porous material with a weak frame. For materials with a weak frame and a micro-structure where the fluid motion relative to the solid frame is very restricted, the speed of sound is close to Wood's value for all frequencies. This behavior is in agreement with the measurements in [22, 24, 27, 32, 36]. For materials with a weak frame and a micro-structure where the fluid motion relative to the solid frame is less restricted, the speed of sound is close to Wood's value for low frequencies and increases with frequency. By parameter fitting we have shown that the Biot model yields a frequency dependence of the speed of sound which is in qualitative agreement with the measurements in [5]. Hence, the Biot equations provide a theoretical framework which can explain the different types of variations of speed of sound that have been obtained in experimentally.

In future research we plan to use micro-structure simulations to investigate how changes in the detailed structure of the parenchyma associated with diseases affect wave propagation properties.

References

[1] J. F. Allard. *Propagation of Sound in Porous Media, Modelling Sound Absorbing Materials*. Elsvier Science Publishers Ltd., 1993.

[2] Ivo Babuška. Error bounds for finite element method. *Numer. Math.*, 16:322–333, 1971.

[3] J. R. Barber. *Elasticity*. Kluwer Academic Publishers, 2002.

[4] A. Bensoussan, J.-L. Lions, and G. C. Papanicolau. Asymptotic analysis for periodic structures. In *Studies in Mathematics and Its Applications*, volume 5. North-Holland, Amsterdam, 1978.

[5] P. J. Berger, E. M. Skuza, C. A. Ramsden, and M. H. Wilkinson. Velocity and attenuation of sound in the isolated fetal lung as it is expanded with air. *J. Appl. Physiol.*, 98:2235–2241, 2005.

[6] M. Biot. Theory of propagation of elstic waves in a fluid-saturated porous solid. I. Low frequency range. *J. Acoust. Soc. Am.*, 28(2):168–178, 1956.

[7] M. Biot. Theory of propagation of elstic waves in a fluid-saturated porous solid. II. Higher frequency range. *J. Acoust. Soc. Am.*, 28(2):179–191, 1956.

[8] M. A. Biot. Generalized theory of acoustic propagation in porous dissipative media. *J. Acoust. Soc. Am.*, 34(9):1254–1264, 1962.

[9] M. A. Biot. Mechanics of deformation and acoustic propagation in porous media. *J. Appl. Phys.*, 33(4):1482–1498, 1962.

[10] M. A. Biot and D. G.Willis. The elastic coefficients of the theory of consolidation. *J. Appl. Mechanics*, 24:594–601, 1957.

[11] S. C. Brenner and L. R. Scott. *The Mathematical Theory of Finite Element Methods*. Springer-Verlag, 1994.

[12] Franco Brezzi. On the existence, uniqueness and approximation of saddle–point problems arising from lagrangian multipliers. *RAIRO Anal. Numér.*, R–2:129–151, 1974.

[13] R. Burridge and J. Keller. Poroelasticity equations derived from microstructure. *J. Acoust. Soc. Am.*, 70(4):1140–1146, 1981.

[14] A. M. Chapman and J. J. L. Higdon. Oscillatory Stokes flow in periodic porous media. *Phys. Fluids A*, 4(10):2099–2116, 1992.

[15] A. M. Chapman and J. J. L. Higdon. Effective elastic properties for a periodic bicontinuous porous medium. *J. Mech. Phys. Solids*, 42(2):283–305, 1994.

[16] P. Göransson. Acoustic a vibrational damping in porous solids. *Phil. Trans. R. Soc. A*, 364:89–108, 2006.

[17] D. Johnson. Recent developments in the acoustic properties of porous medis. In D. Sette, editor, *Frontiers in Physical Acoustics, Proceedings of the International School of Physics Enrico Fermi, Course XCIII*, pages 255–290. North-Holland, Amsterdam, 1986.

[18] D. L. Johnson, J. Koplik, and R. Dashen. Theory of dynamic permeability and tortuosity in fluid-saturated media. *J. Fluid Mech.*, 176:379, 1987.

[19] J. B. Keller. Effective behavior or heterogeneous media. In U. Landman, editor, *Statistical Mechanics and Statistical Methods in Theory and Applications*. Plenum, 1977.

[20] R. C. Kirby and A. Logg. A compiler for variational forms. *ACM Transactions on Mathematical Software*, 32(3):417–444, 2006.

[21] R. C. Kirby and A. Logg. Efficient compilation of a class of variational forms. *ACM Transactions on Mathematical Software*, 33(3), 2007.

[22] S. Kraman. Speed of low-frequency sound through lungs of normal men. *J. Appl. Physiol.*, 55(6):1862–1867, 1983.

[23] S. Lai-Fook and R. Hyatt. Effects of age on elastic moduli of human lungs. *J. Appl. Physiol.*, 89:163–168, 2000.

[24] A. Leung, S. Sehati, D. Young, and C. McLeod. Sound transmission between 50 and 600 Hz in excised pig lungs filled with air and helium. *J. Appl. Physiol.*, 89:2472–2482, 2000.

[25] A. Logg et al. *FFC*, 2006. http://www.fenics.org/ffc/.

[26] A. Logg, G. N. Wells, J. Hoffman, J. Jansson, et al. DOLFIN: A general-purpose finite element library. *http://www.fenics.org/dolfin/*.

[27] M. Mahagnah and N. Gavriely. Gas density does not affect pulmonary acoustic transmission in normal men. *J. Appl. Physiol.*, 78(3):928–937, 1995.

[28] V. N. Oliynik. Features of the "tissue" sound propagation channel in human thorax. *International Journal of Fluid Mechanics Research*, 30(2):187–200, 2003.

[29] V. N. Oliynik. On mechanisms of formation of acoustic properties of pulmonary parenchyma. *International Journal of Fluid Mechanics Research*, 30(4):425–442, 2003.

[30] V. N. Oliynik. Effect of properties of alveolar walls on sound velocity in pulmonary parenchyma. *International Journal of Fluid Mechanics Research*, 33(2):175–85, 2006.

[31] M. R. Owen and M. A. Lewis. The mechanics of lung tissue under high-frequency ventilation. *SIAM J. Appl. Math.*, 61(5):1731–1761, 2001.

[32] R. Paciej, A. Vyshedskiy, J. Shane, and R. Murphy. Transpulmonary speed of sound input into the supraclavicular space. *J. Appl. Physiol.*, 94:604–611, 2003.

[33] H. Pasterkamp, S.S. Kraman, and G.R. Wodicka. Respiratory sounds, advances beyond the stethoscope. *Am. J. Respir. Crit. Care. Med.*, 156:974–987, 1997.

[34] Allan D. Pierce. *Acoustics*. Acoustical Society of America, 1994 edition, 1994.

[35] S. R. Pride, A. F. Gangi, and F. D. Morgan. Deriving the equation of motion for porous isotropic media. *J. Acoust. Soc. Am.*, 92:3278–3290, 1992.

[36] D.A. Rice. Sound speed in pulmonary parenchyma. *J. Appl. Physiol.*, 54(1):304–308, 1983.

[37] E. Sanchez-Palencia. Non-homogeneous media and vibration theory. In *Lecture Notes in Physics 127*. Springer Verlag, New York, 1980.

[38] K. Terada, T. Ito, and N. Kikuchi. Characterization of the mechanical behaviors of solid-fluid mixture by the homogenization method. *Comput. Methods Appl. Mech. Engrg.*, 153:223–257, 1998.

[39] M.-Y. Zhou and P. Sheng. First-principles calculation of dynamic permeability in porous media. *Phys. Rev. B*, 39:12027, 1989.

[40] C. Zwikker and C. W. Kosten. *Sound Absorbing Materials*. Elsevier, 1949.